



# Controlled fabrication of TiO<sub>2</sub>/C<sub>3</sub>N<sub>4</sub> core–shell nanowire arrays: a visible-light-responsive and environmental-friendly electrode for photoelectrocatalytic degradation of bisphenol A

Yajun Wang<sup>1</sup> , Qiaohuan Wu<sup>1</sup> , Yan Li<sup>1</sup> , Liming Liu<sup>1</sup> , Zhouliang Geng<sup>1</sup> , Yuming Li<sup>1</sup> , Juan Chen<sup>1</sup> , Weikun Bai<sup>1</sup> , Guiyuan Jiang<sup>1,\*</sup> , and Zhen Zhao<sup>1</sup>

<sup>1</sup> State Key Laboratory of Heavy Oil Processing, China University of Petroleum, Beijing 102249, China

Received: 22 January 2018

Accepted: 24 April 2018

Published online:

3 May 2018

© Springer Science+Business Media, LLC, part of Springer Nature 2018

## ABSTRACT

Photoelectrocatalytic (PEC) oxidation is a promising method in water treatment due to the synergistic effect of photocatalytic (PC) oxidation and electro-oxidation. Up to now, developing visible-light-responsive, efficient and environmental-friendly electrode for PEC degradation application is still a challenge. In this work, novel and environmental-friendly TiO<sub>2</sub>/C<sub>3</sub>N<sub>4</sub> core–shell nanowire arrays as an electrode were investigated for PEC degradation of bisphenol A (BPA). TiO<sub>2</sub> nanowire arrays provide a direct electron pathway, g-C<sub>3</sub>N<sub>4</sub> serves as a stable and environmental-friendly visible light sensitizer, and effective charge spatial separation can be achieved across the well-matched core–shell interface. Compared with TiO<sub>2</sub> nanowire arrays, TiO<sub>2</sub>/C<sub>3</sub>N<sub>4</sub> core–shell nanowire arrays exhibit higher PC and PEC performance. The photocurrent response of the TiO<sub>2</sub> nanowire arrays is enhanced about two times after C<sub>3</sub>N<sub>4</sub> shell deposition. And the PEC performance of TiO<sub>2</sub>/C<sub>3</sub>N<sub>4</sub> core–shell nanowire arrays is significantly enhanced, which is one time higher than that of TiO<sub>2</sub> (under 1.0 V external potential). The enhancement of PEC performance of TiO<sub>2</sub> nanowire arrays after C<sub>3</sub>N<sub>4</sub> modification can be attributed to the synergistic photoelectric effect, well-matched interface and efficient charge separation induced by the type-II TiO<sub>2</sub>/C<sub>3</sub>N<sub>4</sub> band alignment. Moreover, the intermediate products of BPA degradation by PEC oxidation were analyzed by gas chromatography–mass spectrometry and five specific products were identified, and then two possible pathways for BPA degradation by PEC process were proposed.

Address correspondence to E-mail: jianggy@cup.edu.cn

## Introduction

With the development of the industrialization, the environment pollution has become one of the major concerns of the international community. Photocatalytic (PC) oxidation is considered as a promising way to degrade environment pollutant due to its high oxidation ability and broad compound applicability [1, 2]. As an enhanced photocatalysis technique, photoelectrocatalytic (PEC) oxidation has been proven to be an efficient method that can greatly enhance the PC oxidation activity by exploiting the synergism between PC oxidation and electro-oxidation [3–8]. Moreover, photocatalyst immobilized on a conductive substrate as an electrode is more practical than that in a powdery form for industrial application.

TiO<sub>2</sub> is the most widely used photocatalyst due to its high oxidation ability, high resistance to photocorrosion, high chemical stability, non-toxic and low cost [9–11]. However, the low quantum efficiency, poor visible light response and separation problems greatly limit the large-scale industrial application of TiO<sub>2</sub> nanoparticles [9]. Many kinds of TiO<sub>2</sub> films on various substrates were used to replace TiO<sub>2</sub> nanoparticles as photocatalyst. Compared with TiO<sub>2</sub> film, TiO<sub>2</sub> nanowire arrays as one-dimensional (1D) nanostructures are expected to have higher photocatalytic activity due to their large surface-to-volume ratios, rapid charge transport and recyclable characteristics [12–14]. To extend the application of TiO<sub>2</sub> nanowire arrays, considerable efforts have been devoted to improve the photogenerated charge separation efficiency and extend the light response range, such as element doping [15, 16], noble metal deposition [17, 18] and semiconductor coupling [19–24].

Coupling TiO<sub>2</sub> nanowires with another narrow bandgap semiconductor is an effective way to utilize visible light and enhance photocatalytic activity. Currently, chalcogenide materials (such as CdS, CdSe and ZnSe) are preferred and mostly used narrow bandgap semiconductor to combine with TiO<sub>2</sub> nanowires due to their visible light absorption ability and suitable band position [19–22]. However, chalcogenide materials always suffer photocorrosion and instability in the PEC reaction, leading to a leakage of heavy metal, which is harmful to environmental remediation. Therefore, it is urgent to develop a visible-light-responsive, efficient and

environment-friendly electrode for PEC degradation application. Graphitic carbon nitride (g-C<sub>3</sub>N<sub>4</sub>) with a bandgap of 2.7 eV is the most stable allotrope of carbon nitride and is a metal-free semiconductor [25, 26]. It has attracted extensive scientific interest due to its high chemical stability and visible light absorption ability. G-C<sub>3</sub>N<sub>4</sub> has been widely employed in the degradation of dye, phenol and other pollutants [27, 28]. Coupling g-C<sub>3</sub>N<sub>4</sub> with wide bandgap semiconductors with more positive conduction band is an effective way to fabricate efficient and visible-light-responsive photocatalysts. Many g-C<sub>3</sub>N<sub>4</sub>-based composites such as ZnO/C<sub>3</sub>N<sub>4</sub> [29], Bi<sub>2</sub>WO<sub>6</sub>/C<sub>3</sub>N<sub>4</sub> [30], ZnWO<sub>4</sub>/C<sub>3</sub>N<sub>4</sub> [31] have been reported and shown enhanced photocatalytic performance. The combination of TiO<sub>2</sub> and g-C<sub>3</sub>N<sub>4</sub> may be an ideal system to achieve an enhanced charge separation and transfer due to the matched band alignment between TiO<sub>2</sub> and g-C<sub>3</sub>N<sub>4</sub>. Moreover, the visible-light-responsive capacity, chemical stability and environmental-friendly structure make g-C<sub>3</sub>N<sub>4</sub> an excellent candidate in PEC degradation application. Actually, some TiO<sub>2</sub>/g-C<sub>3</sub>N<sub>4</sub> combination works were developed and shown promising results [32–35]. Zhu and co-workers synthesized a C<sub>3</sub>N<sub>4</sub>/TiO<sub>2</sub> hybrid photocatalyst with highly improved photocatalytic activity via a ball milling method [34]. Wang and co-workers synthesized a macro-/mesoporous g-C<sub>3</sub>N<sub>4</sub>/TiO<sub>2</sub> composite and found that g-C<sub>3</sub>N<sub>4</sub>/TiO<sub>2</sub> presented a higher photocatalytic activity than pure TiO<sub>2</sub> and g-C<sub>3</sub>N<sub>4</sub>. The enhanced photocatalytic performance was attributed to the heterojunction between TiO<sub>2</sub> and g-C<sub>3</sub>N<sub>4</sub>, as well as the high surface area [32]. However, to the best of our knowledge, there is no report regarding the fabrication and application of TiO<sub>2</sub>/g-C<sub>3</sub>N<sub>4</sub> core-shell nanowire arrays electrode in the PEC degradation although it has many unique merit in environmental application. Moreover, the core-shell structure with proper band alignment and well-matched interface can achieve the selective isolation of charge carriers by spatial separation of electrons and holes across the core-shell interface, thus suppressing the charge recombination.

Herein, we report our efforts in fabricating TiO<sub>2</sub>/g-C<sub>3</sub>N<sub>4</sub> (denoted as TiO<sub>2</sub>/C<sub>3</sub>N<sub>4</sub>) core-shell nanowire arrays and exploring the application of this TiO<sub>2</sub>/C<sub>3</sub>N<sub>4</sub> electrode in PEC degradation of bisphenol A (BPA). These TiO<sub>2</sub>/C<sub>3</sub>N<sub>4</sub> core-shell nanowire arrays were synthesized via a hydrothermal method followed by a chemical vapor deposition (CVD)

method. TiO<sub>2</sub> nanowire arrays provide a direct electron pathway, and g-C<sub>3</sub>N<sub>4</sub> serves as a photo-sensitizer; the type-II band alignment and the well-matched core-shell structure of TiO<sub>2</sub> and g-C<sub>3</sub>N<sub>4</sub> can facilitate the photogenerated charge separation and transfer. BPA was chosen as a model pollutant to investigate the PC and PEC activity of as-prepared samples. BPA is one of the priority endocrine disrupting compounds which should be monitored and controlled due to its large-scale production and extensive applications. Many research reports point out that even very low level of BPA may cause infertility as well as breast, ovarian and testicular cancer of human and wildlife [36, 37]. TiO<sub>2</sub>/C<sub>3</sub>N<sub>4</sub> core-shell nanowire arrays show superior BPA degradation activity than pure TiO<sub>2</sub> nanowire arrays. The effect of external potential on PEC degradation of BPA, the identification of BPA degradation intermediate products and the possible degradation pathway were systematically investigated.

## Experimental

### Preparation of the TiO<sub>2</sub> nanowire arrays and TiO<sub>2</sub>/C<sub>3</sub>N<sub>4</sub> core-shell nanowire arrays

**Preparation of TiO<sub>2</sub> nanowire arrays:** The TiO<sub>2</sub> nanowire arrays on a carbon cloth were prepared using a hydrothermal method according to a previous report [38]. Firstly, the carbon cloth was cleaned by sonication in acetone and methanol, subsequently rinsed with deionized (DI) water and finally dried in a nitrogen stream. The carbon cloth was placed within a sealed Teflon reactor (200 mL), containing 100 mL of toluene, 10 mL of tetrabutyl titanate, 10 mL of titanium tetrachloride (1 M in toluene) and 10 mL of hydrochloric acid (37 wt%). The Teflon reactor was kept in an oven at 180 °C for 22 h. After cooling down to room temperature, the carbon cloth was taken out, then rinsed with ethanol and DI water, and finally annealed in air at 500 °C for 2 h.

**Preparation of TiO<sub>2</sub>/C<sub>3</sub>N<sub>4</sub> core-shell nanowire arrays:** Deposition of g-C<sub>3</sub>N<sub>4</sub> onto the TiO<sub>2</sub> nanowire was performed by a CVD process, and melamine was used as a precursor. Firstly, 2.0 g melamine was added in the bottom of a ceramic crucible with a cover, and a carbon cloth with pre-grown TiO<sub>2</sub> nanowire was placed on the upper position of the crucible. Then, the crucible was heated at 550 °C for

4 h with a temperature rise rate at 5 °C/min in a muffle furnace. After cooling down to room temperature, the as-prepared samples were rinsed with ethanol and DI water to remove the g-C<sub>3</sub>N<sub>4</sub> attaching to the carbon cloth. In the bottom of the crucible, g-C<sub>3</sub>N<sub>4</sub> powders can also be obtained.

### Characterization

X-ray diffraction patterns were measured by X-ray diffraction with Cu K $\alpha$  radiation ( $\lambda = 1.5406 \text{ \AA}$ ) on a Shimadzu XRD 6000 diffractometer. Morphologies of the as-prepared photocatalysts were characterized by scanning electron microscopy (SEM) and transmission electron microscopy (TEM). SEM images were investigated with a FEI Quanta 200F microscope at an accelerating voltage of 30 kV. TEM and high-resolution transmission electron microscopy (HRTEM) were performed on a JEOL JEM-2100 microscope with an accelerating voltage of 120 kV. The UV-vis diffuse reflectance spectroscopy (DRS) was obtained by a UV-vis spectrophotometer (Hitachi U-4100) with the integration sphere diffuse reflectance attachment, using BaSO<sub>4</sub> as the reference. X-ray photoelectron spectroscopy (XPS) spectra were carried out on a K-Alpha XPS instrument. The concentration of BPA during the reaction was examined by a high-performance liquid chromatography (HPLC) on a Agilent 1200 UPLC system with the following conditions: column, 100 mm BEH C18 column; detector, UV detector operated at 280 nm; mobile phase, 1 mL/min of methanol and water (70/30, v/v); injection volume of BPA, 5  $\mu$ L. The intermediate products of the PEC degradation of BPA were identified by gas chromatography-mass spectrometry (GC/MS) on a Bruker (ACION TQ, USA) combined with an Agilent DB (30  $\times$  0.25 mm, 0.25  $\mu$ m) quartz capillary column and an electron impact (EI) detector (70 eV). The initial temperature of column oven was 40 °C and held for 1 min; then, it increased up to 280 °C with a heating rate of 15 °C/min and held for 8 min. The temperatures were set as follows: injection port, 260 °C; interface, 250 °C; ion source, 230 °C. Helium was used as a carrier gas with a flow rate of 1 mL/min.

## Photoelectrocatalysis experiments

The photoelectrochemical measurements and PEC reactions were performed in a rectangular reactor using a CHI 660E (Shanghai, China) electrochemical workstation. A standard three-electrode cell system was used in the photoelectrochemical measurements and PEC reactions, including a Pt counter electrode, a working electrode ( $\text{TiO}_2/\text{C}_3\text{N}_4$  core-shell nanowire arrays, active area of  $2 \times 2 \text{ cm}^2$ ) and a reference electrode (a saturated calomel electrode, SCE). The  $\text{TiO}_2/\text{C}_3\text{N}_4$  core-shell nanowire arrays electrode was irradiated with visible light obtained from a 300 W Xe lamp (PLS-SXE300C/300CUV, Perfect Light, Beijing) with 420-nm cutoff filter. The average visible light intensity was  $100 \text{ mW cm}^{-2}$ . An electrolyte solution with a concentration of  $0.1 \text{ mol L}^{-1} \text{ Na}_2\text{SO}_4$  was used in the photoelectrochemical measurements. Photocurrent responses were investigated at 0.0 V (with reference to the SCE) under light-on and light-off cycles. The electrochemical impedance spectra (EIS) were performed in the frequency range of 100 kHz–0.01 Hz with an amplitude of the sinusoidal wave of 5 mV. The PC and PEC performance of the as-prepared samples was measured by the removal of BPA (with an initial concentration of  $10 \text{ mg L}^{-1}$ ) in 200 mL  $\text{Na}_2\text{SO}_4$  ( $0.1 \text{ mol L}^{-1}$ ) solution. The main oxidative species in the PEC process of the  $\text{TiO}_2/\text{C}_3\text{N}_4$  core-shell nanowire arrays were detected through trapping experiment by addition of hole scavenger (methanol), hydroxyl radical scavenger (tert-butyl alcohol, t-BuOH) and superoxide radical scavenger (benzoquinone, BQ).

## Results and discussion

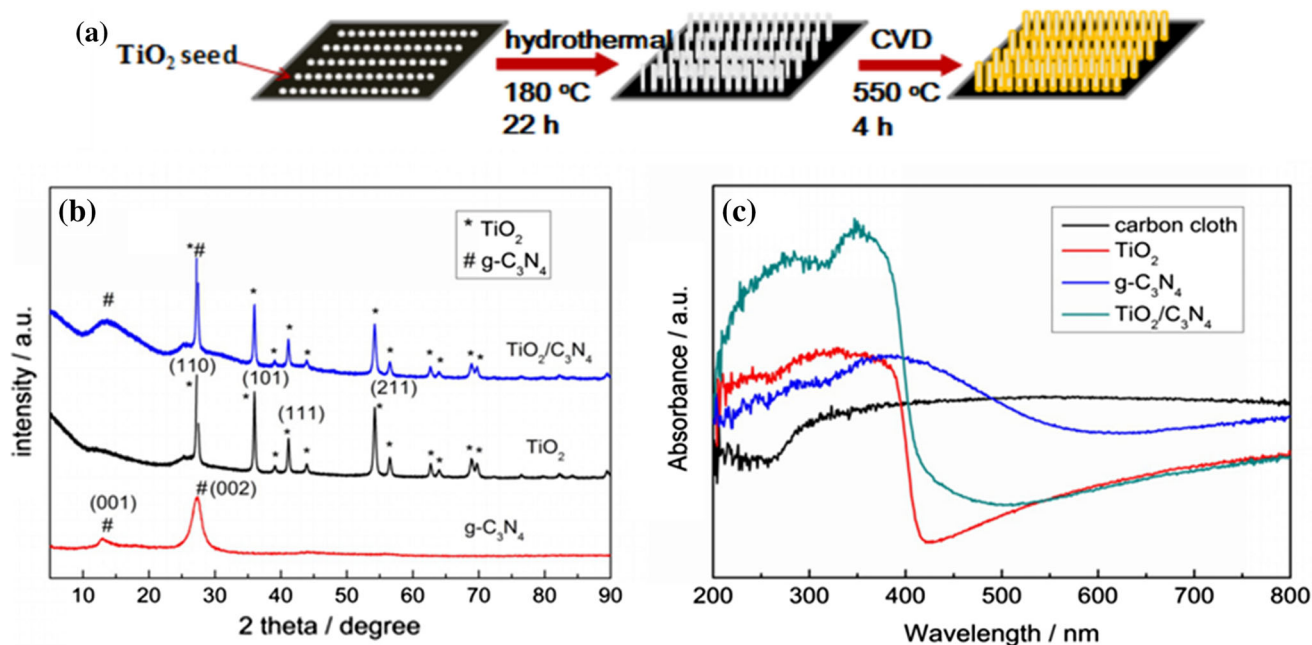
### Catalyst characterization

Figure 1a shows the two-step fabrication process of  $\text{TiO}_2/\text{C}_3\text{N}_4$  core-shell nanowire arrays grown on carbon cloth. Firstly, the  $\text{TiO}_2$  nanowire arrays were grown on the carbon cloth substrate by hydrothermal method. Then, the  $\text{C}_3\text{N}_4$  shell was deposited on the surface of  $\text{TiO}_2$  nanowires via CVD method using melamine as a precursor. The XRD patterns of  $\text{TiO}_2$ ,  $\text{C}_3\text{N}_4$  and  $\text{TiO}_2/\text{C}_3\text{N}_4$  core-shell nanowire arrays are shown in Fig. 1b. Diffraction peaks appearing in the pure  $\text{TiO}_2$  nanowires can be well indexed to the rutile  $\text{TiO}_2$  (JCPDS.21-1276). Pure  $\text{C}_3\text{N}_4$  shows two

characteristic peaks at  $12.9^\circ$  and  $27.3^\circ$ , which can be attributed to the interplanar separation (100) and the stacking of the conjugated aromatic system (002) (JCPDS 87-1526) [39, 40]. The  $\text{TiO}_2/\text{C}_3\text{N}_4$  core-shell nanowire arrays exhibit all the characteristic peaks of rutile  $\text{TiO}_2$ , suggesting that the crystal phase of  $\text{TiO}_2$  does not change after deposited with  $\text{C}_3\text{N}_4$  shell. It is worth to point out that the peak of (002) planar of g- $\text{C}_3\text{N}_4$  at  $27.3^\circ$  overlaps with the (110) planar peak of rutile  $\text{TiO}_2$ . Nevertheless, the characteristic peaks of g- $\text{C}_3\text{N}_4$  at  $12.9^\circ$  can be observed in the XRD pattern of  $\text{TiO}_2/\text{C}_3\text{N}_4$  core-shell nanowire arrays, indicating that the g- $\text{C}_3\text{N}_4$  was successfully deposited on the  $\text{TiO}_2$  nanowires. The optical properties of the  $\text{TiO}_2$ ,  $\text{C}_3\text{N}_4$  and  $\text{TiO}_2/\text{C}_3\text{N}_4$  core-shell nanowire arrays were examined by UV-vis DRS spectra, and the results are shown in Fig. 1c. Pure  $\text{TiO}_2$  nanowires show a sharp absorption edge rise at around 410 nm, which corresponds to a band gap of 3.0 eV. The pure  $\text{C}_3\text{N}_4$  displays a characteristic absorption rise at around 550 nm, corresponding to a band gap of 2.3 eV. Compared with that of pure  $\text{TiO}_2$ , the absorption edge of  $\text{TiO}_2/\text{C}_3\text{N}_4$  nanowires was extended to the visible light range due to the presence of  $\text{C}_3\text{N}_4$ , which is beneficial for the solar energy utilization.

The structural morphology of  $\text{TiO}_2$  and  $\text{TiO}_2/\text{C}_3\text{N}_4$  nanowire arrays was examined by SEM analysis (Fig. 2). Figure 2a, b shows the SEM images of  $\text{TiO}_2$  nanowire arrays grown on the carbon cloth. The inset of Fig. 2a is pure carbon cloth. As can be seen, the high-density and orderly  $\text{TiO}_2$  nanowire arrays were grown uniformly on the carbon cloth. These  $\text{TiO}_2$  nanowires with smooth surface are about 30–50 nm in diameter (Fig. 2b). The CVD method was performed to deposit the  $\text{C}_3\text{N}_4$  shell on the pre-grown  $\text{TiO}_2$  nanowires. Figure 2c shows a large-scale SEM image of the  $\text{TiO}_2/\text{C}_3\text{N}_4$  core-shell nanowire arrays, which indicates that the structure of  $\text{TiO}_2$  nanowires do not obviously change after  $\text{C}_3\text{N}_4$  deposition. From the high-magnification SEM image of  $\text{TiO}_2/\text{C}_3\text{N}_4$  nanowire (Fig. 2d), a shell deposited on the surface of the  $\text{TiO}_2$  nanowire can be clearly observed. The surfaces of the  $\text{TiO}_2$  nanowires become rough, and the diameters of the  $\text{TiO}_2$  nanowires increase up to the range of 80–100 nm after deposited with  $\text{C}_3\text{N}_4$ . As can be seen, the high-density and orderly  $\text{TiO}_2/\text{C}_3\text{N}_4$  core-shell nanowires were successfully synthesized.

The HRTEM images of  $\text{TiO}_2/\text{C}_3\text{N}_4$  core-shell nanowires confirm that  $\text{TiO}_2$  nanowire is covered by



**Figure 1** a Fabrication process of TiO<sub>2</sub>/C<sub>3</sub>N<sub>4</sub> core–shell nanowire arrays; b the XRD patterns of TiO<sub>2</sub>, C<sub>3</sub>N<sub>4</sub> and TiO<sub>2</sub>/C<sub>3</sub>N<sub>4</sub> core–shell nanowire arrays; c the UV–vis DRS spectra of TiO<sub>2</sub>, C<sub>3</sub>N<sub>4</sub> and TiO<sub>2</sub>/C<sub>3</sub>N<sub>4</sub> core–shell nanowire arrays.

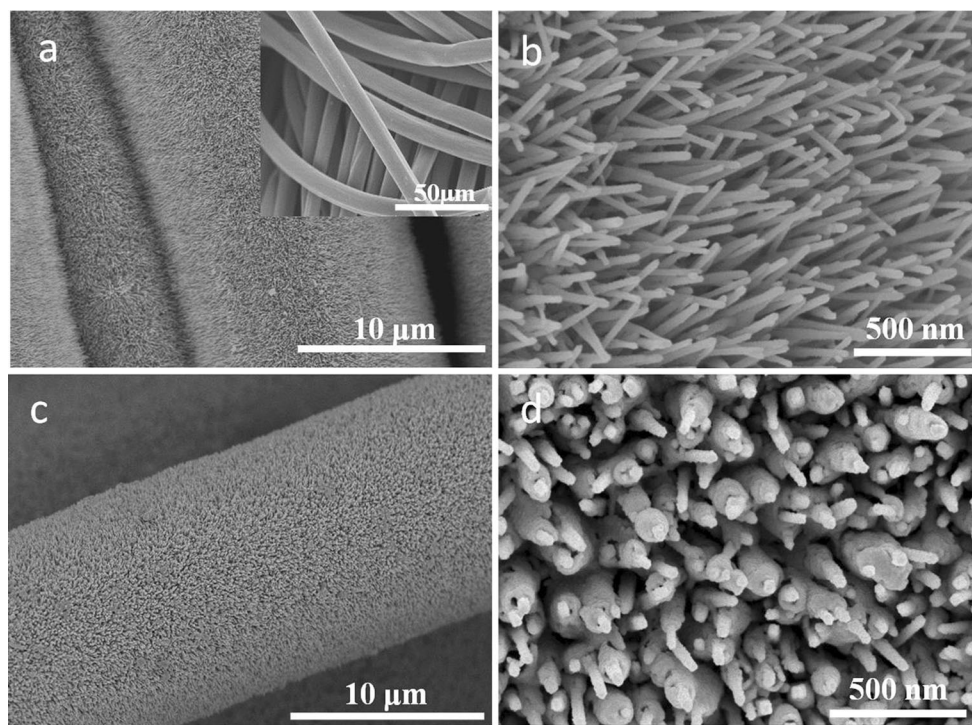


**Figure 2** SEM images of TiO<sub>2</sub> nanowire arrays (a, b) and TiO<sub>2</sub>/C<sub>3</sub>N<sub>4</sub> core–shell nanowire arrays (c, d); inset of (a): the pure carbon cloth.

a thin layer of C<sub>3</sub>N<sub>4</sub> (Fig. S1). The diameter of TiO<sub>2</sub> nanowire is about 30 nm, which is consistent with the SEM results. And the measured interplanar spacing

of TiO<sub>2</sub> is 0.325 nm, which matches well with the rutile TiO<sub>2</sub> (110) plane. The measured interplanar spacing of 0.320 nm in the deposition layer is

correlated with the (002) crystal planes of  $C_3N_4$ , further confirming the deposition of  $C_3N_4$ .

The XPS measurement was performed to investigate the surface composition and chemical states of  $TiO_2$  and  $TiO_2/C_3N_4$  nanowire arrays. Figure 3 shows the XPS survey spectra and magnified spectra of N 1s, C 1s, Ti 2p and O 1s. As can be seen from Fig. 3a,  $TiO_2$  nanowire arrays are composed of C, Ti, O, whereas  $TiO_2/C_3N_4$  core-shell nanowire arrays are composed of C, Ti, O and N, indicating the formation of  $C_3N_4$  in the  $TiO_2/C_3N_4$  nanowire arrays. In the magnified N 1s spectra of  $TiO_2/C_3N_4$  nanowire arrays (Fig. 3b), a broad peak extending from 395 to 406 eV can be observed. Three peaks can be distinguished to be centered at 398.3, 400.3, 404.0 eV, respectively. The main peak at 398.3 eV can be attributed to the  $sp^2$ -hybridized nitrogen ( $N=C=N$ ), indicating the presence of  $sp^2$ -bonded  $C_3N_4$ . The other two peaks at 400.3 and 404.0 eV can be assigned to the nitrogen in tertiary  $N-(C)_3$  groups and the charging effects [41, 42]. Figure 3c shows the C 1s features of  $TiO_2/C_3N_4$  core-shell nanowire arrays. The peak at 284.1 eV is assigned to the C-C group due to the carbon contamination. And the peak at 288.0 eV is attributed to the  $N=C=N$  group in the graphitic  $C_3N_4$  [39, 40]. From the Ti 2p spectrum of  $TiO_2/C_3N_4$  nanowire arrays (Fig. 3d), two peaks at

binding energy of 458.3 eV ( $Ti\ 2p_{3/2}$ ) and 464.0 eV ( $Ti\ 2p_{1/2}$ ) can be observed [43]. As can be seen from Fig. 3e, the O 1s peak at binding energy of 529.6 and 531.2 eV can be attributed to the  $O^{2-}$  in the sample and the  $-OH$  group of water molecules on the surface of the sample, respectively [44]. The XPS spectra further confirm the presence of the  $C_3N_4$ .

### Photoelectrochemical properties

Photoelectrochemical experiments were carried out in a standard three-electrode system. The photocurrent responses of  $TiO_2$  nanowire arrays and  $TiO_2/C_3N_4$  core-shell nanowire arrays were investigated with light-on and light-off cycles at a bias potential of 0 V versus SCE electrode, and the results are shown in Fig. 4a. Fast and steady photocurrent responses are observed for each light-on and light-off cycle in  $TiO_2$  and  $TiO_2/C_3N_4$  electrodes, indicating that the electrodes have good chemical stability and photo-stability. The photocurrent response of carbon cloth was also investigated for comparison, and no photocurrent response can be observed. Under visible light irradiation, the photocurrent density of the pure  $TiO_2$  is  $0.0025\text{ mA/cm}^2$ . Meanwhile, the photocurrent density of the  $TiO_2/C_3N_4$  is  $0.0075\text{ mA/cm}^2$ , which is three times of that of pure  $TiO_2$ . The photocurrent

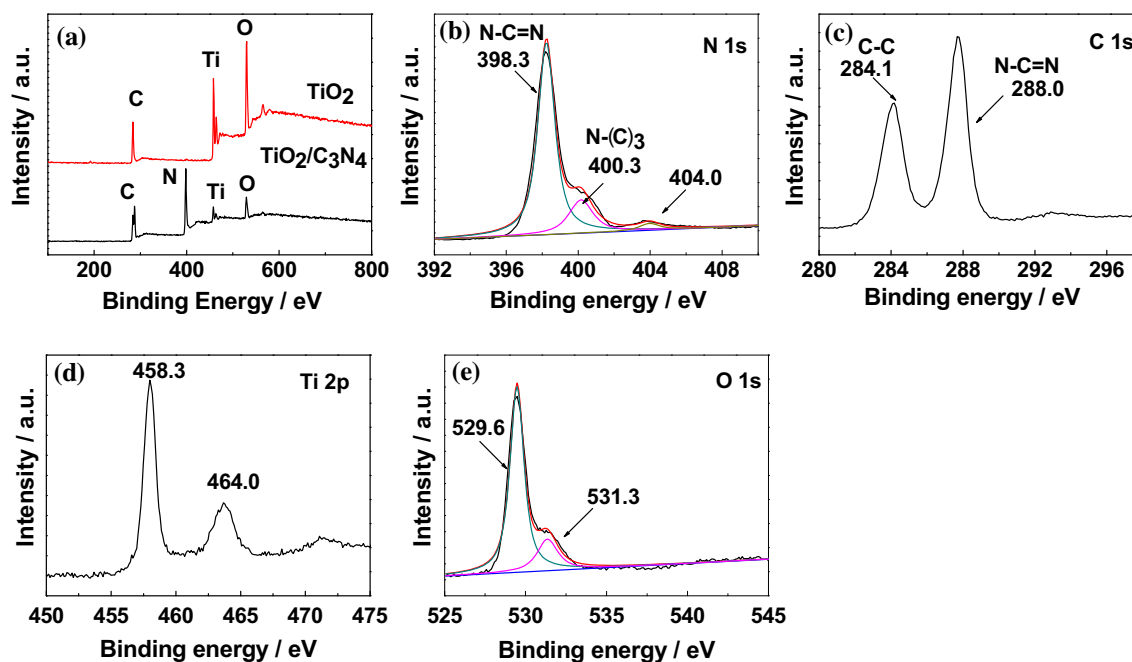


**Figure 3** XPS survey spectra of  $TiO_2$  and  $TiO_2/C_3N_4$  nanowire arrays (a); magnified spectra of **b** N 1s peaks, **c** C 1s peaks, **d** Ti 2p peaks and **e** O 1s peaks of  $TiO_2/C_3N_4$  core-shell nanowire arrays.

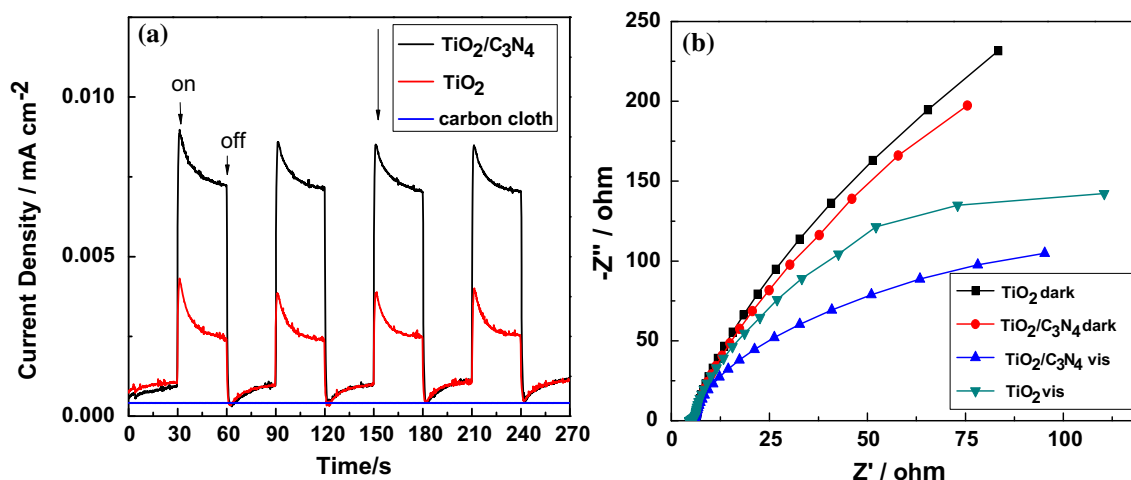


**Figure 4** Photocurrent responses (a) and EIS Nyquist plots (b) of TiO<sub>2</sub> nanowire arrays and TiO<sub>2</sub>/C<sub>3</sub>N<sub>4</sub> core–shell nanowire arrays under visible light irradiation,  $\lambda \geq 420$  nm.

enhancement of the TiO<sub>2</sub>/C<sub>3</sub>N<sub>4</sub> electrode suggests a higher charge separation efficiency, which is beneficial for the BPA PC and PEC degradation process. EIS is a powerful approach to investigate the resistance of the electrodes, which indicates the charge separation process in electrodes [9, 45]. Figure 4b displays the EIS Nyquist plots of the TiO<sub>2</sub> and TiO<sub>2</sub>/C<sub>3</sub>N<sub>4</sub> electrodes with and without visible light irradiation. The radius of the arc in the EIS spectra indicates the charge separation and transfer resistance at the electrode; the smaller the radius, the higher the charge separation efficiency [9, 30, 45]. The TiO<sub>2</sub>/C<sub>3</sub>N<sub>4</sub> electrodes show smaller radius of the arc than pure TiO<sub>2</sub> with and without visible light irradiation, suggesting an improved charge separation and transfer process in TiO<sub>2</sub>/C<sub>3</sub>N<sub>4</sub>. The results of photoelectrochemical characterization indicate that the C<sub>3</sub>N<sub>4</sub> modification can effectively enhance the photogenerated charge separation efficiency of the TiO<sub>2</sub> nanowires.

### Enhancement of PC and PEC activity

The BPA PC and PEC degradation experiment was performed under visible light irradiation ( $\lambda \geq 420$  nm). Figure 5a shows the PC and PEC activity of TiO<sub>2</sub>, C<sub>3</sub>N<sub>4</sub> and TiO<sub>2</sub>/C<sub>3</sub>N<sub>4</sub>, and the apparent rate constant  $k$  is shown in the inset graph. As is well known, the PC and PEC degradation processes obey pseudo-first-order kinetics; the slope of the linear line in the plots of  $\ln(C/C_0)$  of BPA versus irradiation time ( $t$ ) represents the apparent rate constant  $k$  [46, 47]. The electro-oxidation of BPA at 1.0 V

versus SCE electrode and visible light photolysis (in the absence of the photocatalyst) were performed as references. As can be seen, the visible light photolysis (in the absence of the photocatalyst) has no obvious effect on BPA removal. The TiO<sub>2</sub>/C<sub>3</sub>N<sub>4</sub> shows much higher PEC activity than pure TiO<sub>2</sub> and C<sub>3</sub>N<sub>4</sub>. The rate constant  $k$  of PEC degradation of TiO<sub>2</sub>/C<sub>3</sub>N<sub>4</sub> under 1.0 V external potential is 0.00411 min<sup>-1</sup>, which is one time higher than that of pure TiO<sub>2</sub> (0.00203 min<sup>-1</sup>). Moreover, the reaction rate constant  $k$  of PEC degradation of TiO<sub>2</sub>/C<sub>3</sub>N<sub>4</sub> is larger than the sum of the electro-oxidation and PC degradation, suggesting a synergetic effect between electro-oxidation and PC degradation in the PEC process. The effect of the external potential on the PEC degradation of BPA of TiO<sub>2</sub>/C<sub>3</sub>N<sub>4</sub> was investigated, and the results are shown in Fig. 5b. As can be seen, the PEC activity first increases and then decreases with the increasing external potential. The TiO<sub>2</sub>/C<sub>3</sub>N<sub>4</sub> core–shell nanowire arrays present highest PEC activity (apparent rate constant  $k = 0.01041$  min<sup>-1</sup>) at external potential of 2 V. When the external potential is higher than 2 V, the high external potential may induce fast electro-polymerization of BPA, which would block the current transfer and destroy the synergetic effect of the system, leading to a decreased PEC activity.

### Identification of intermediate products and the possible degradation pathway

The identity of the intermediate products from the degradation of BPA was monitored by HPLC and GC–MS. The intermediate products are shown in

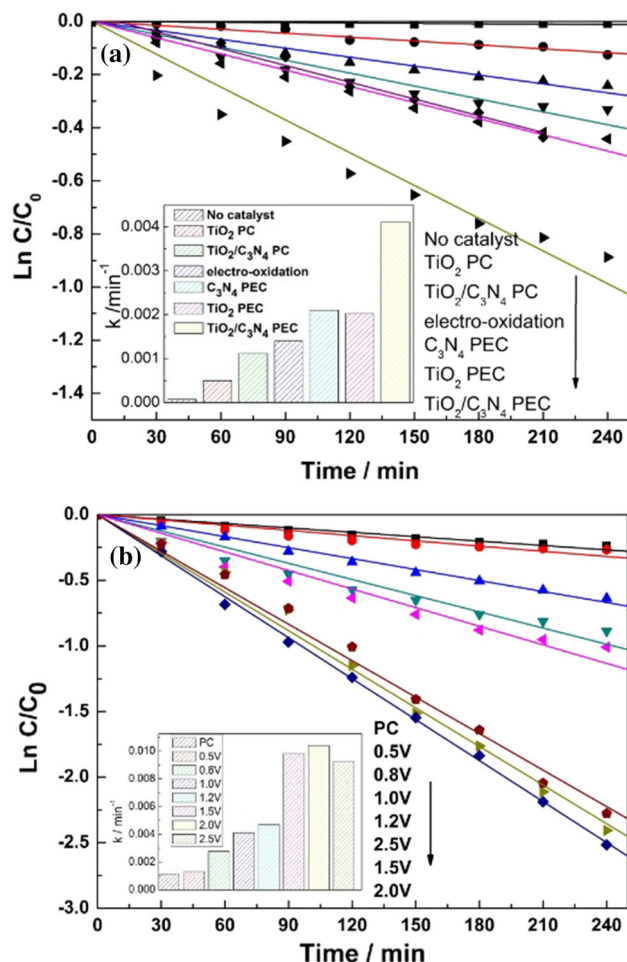


**Figure 5** Comparison of electro-oxidation, PC and PEC degradation rate of BPA a ( $\lambda \geq 420$  nm, external potential = 1.0 V), and comparison of the degradation rate of BPA over  $\text{TiO}_2/\text{C}_3\text{N}_4$  core-shell nanowire arrays under different external potentials ( $\lambda \geq 420$  nm).

Table S1, and the possible BPA degradation pathway in PEC process is proposed in Fig. 6. Five main intermediates were identified as 3-pentanone, p-isopropenyl phenol, 1-(4-benzyl alcohol) ethanone, (1,1'-phenyl) ethylene and (2-methyl-1-phenyl-1-propenyl) benzene. Based on these intermediates, the possible degradation pathway of BPA was proposed, including dehydroxylation, cleavage of C–C bonds, elimination reactions and oxidation [48, 49]. As can be seen from Fig. 6, the degradation of BPA in PEC process can be divided into two possible pathways according to the bonds broken and the previously reported results [48, 49]. The first one is dehydroxylation; the bonds connecting two hydroxyl groups with aromatic rings in BPA are first cleaved, leading to the formation of (2-methyl-1-phenyl-1-propenyl)

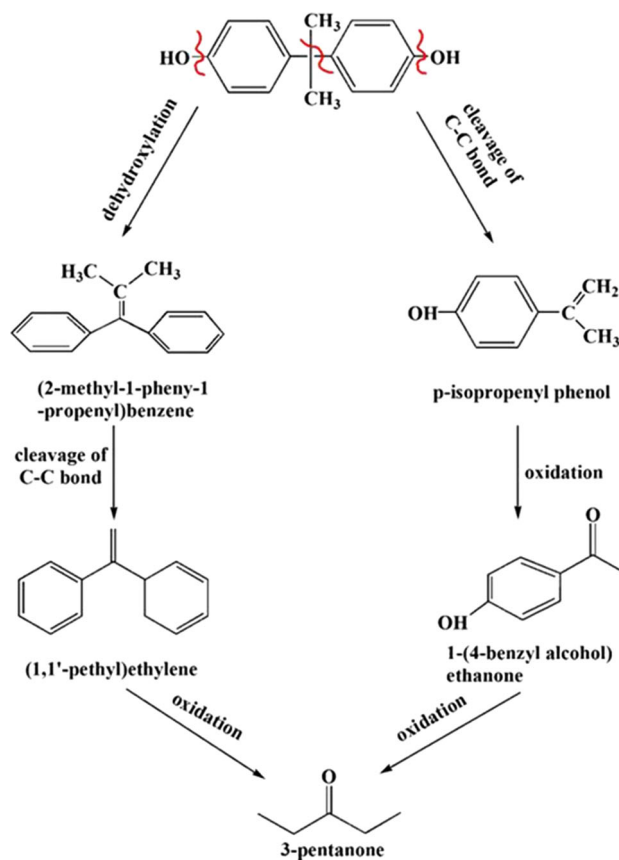


**Figure 6** Proposed BPA degradation pathway by  $\text{TiO}_2/\text{C}_3\text{N}_4$  core-shell nanowire arrays.

benzene. Then, (2-methyl-1-phenyl-1-propenyl) benzene is subsequently oxidized to form (1, 1'-phenyl) ethylene. Furthermore, the C–C bond connecting the two aromatic rings is vulnerable because of the two electron-donating hydroxyl groups. Therefore, the second pathway is the cleavage of the C–C bond connecting two aromatic rings in BPA, resulting in the formation of p-isopropenyl phenol. The p-isopropenyl phenol can be degraded to p-hydroxyacetophenone. These intermediates are further oxidized to generate 3-pentanone, which can be further oxidized by radicals.

### Mechanism of enhancement of PEC activity

The identification of main oxidative species is important to reveal the mechanism of the synergistic effect of  $\text{TiO}_2/\text{C}_3\text{N}_4$ . Generally, three oxidative species, hydroxyl radical, hole and superoxide radical, are hypothesized to be involved in photocatalysis reaction. The main oxidative species were detected through the trapping experiments by adding hole



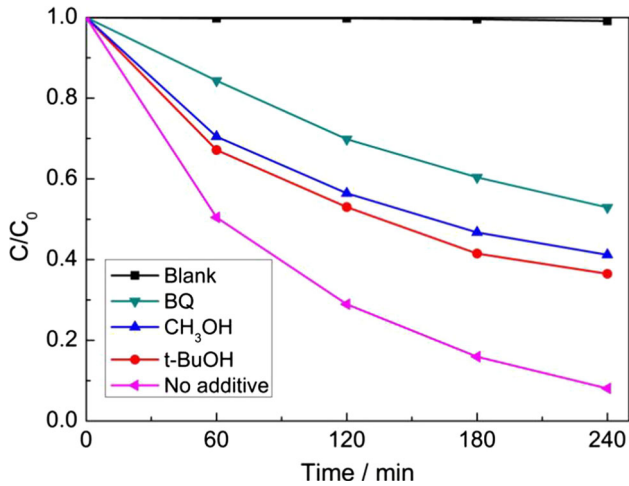


**Figure 7** Plots of photogenerated carriers trapping on PEC process by TiO<sub>2</sub>/C<sub>3</sub>N<sub>4</sub> under 2.0 V external potential and visible light irradiation ( $\lambda \geq 420$  nm).

scavenger (methanol) [50], hydroxyl radical scavenger (t-BuOH) [29, 51] and superoxide radical scavenger (BQ) [43], respectively. The results are shown in Fig. 7. The addition of a scavenger of superoxide radicals (BQ) obviously decreases the PEC activity of TiO<sub>2</sub>/C<sub>3</sub>N<sub>4</sub>, indicating that superoxide radicals are the main oxidative species in the BPA degradation. The addition of methanol and t-BuOH reduces the PEC activity of TiO<sub>2</sub>/C<sub>3</sub>N<sub>4</sub> in a certain extent, suggesting that hole and hydroxyl radical are part of oxidative species.

Based on the above results, a schematic diagram of the possible mechanism of the charge transfer process of the TiO<sub>2</sub>/C<sub>3</sub>N<sub>4</sub> core-shell nanowire array is shown in Fig. 8. The position of valance band (VB) and conduction band (CB) of C<sub>3</sub>N<sub>4</sub> is higher than that of TiO<sub>2</sub> according to the reported results [33]. The

suitable valence band and conduction band position of TiO<sub>2</sub> and C<sub>3</sub>N<sub>4</sub> can form a type-II structure, which can lead to a spatial separation of the electrons and holes on TiO<sub>2</sub> and C<sub>3</sub>N<sub>4</sub> heterojunction [52], resulting in an enhanced charge separation efficiency. The TiO<sub>2</sub> itself cannot be excited by visible light, but C<sub>3</sub>N<sub>4</sub> can absorb visible light to generate electrons and holes. Therefore, under visible light irradiation, the excited electrons of the CB of C<sub>3</sub>N<sub>4</sub> would inject into the CB of TiO<sub>2</sub> due to the type-II structure. The electrons would be subsequently driven to the counter electrode by the external potential, leaving the holes on the C<sub>3</sub>N<sub>4</sub> shell, resulting in an improved charge separation and transfer process. The electrons and holes would subsequently react with water and oxygen to produce active superoxide and hydroxyl radicals. The holes and radicals would participate in the degradation of BPA and its intermediate products, leading to a visible light activity of TiO<sub>2</sub>/C<sub>3</sub>N<sub>4</sub> core-shell nanowire arrays. Moreover, the synergistic effect of PC and electro-oxidation can further enhance the activity of TiO<sub>2</sub>/C<sub>3</sub>N<sub>4</sub>. The applied external potential not only can enhance the charge separation efficiency by driving the electrons to the counter electrode, but also can directly degrade the BPA.

### Conclusions

In summary, novel TiO<sub>2</sub>/C<sub>3</sub>N<sub>4</sub> core-shell nanowire arrays were successfully prepared via a hydrothermal method followed by a CVD method. TiO<sub>2</sub>/C<sub>3</sub>N<sub>4</sub> core-shell nanowire arrays served as a working electrode, which was applied to PEC degradation of BPA. TiO<sub>2</sub> nanowire arrays provide a direct electron

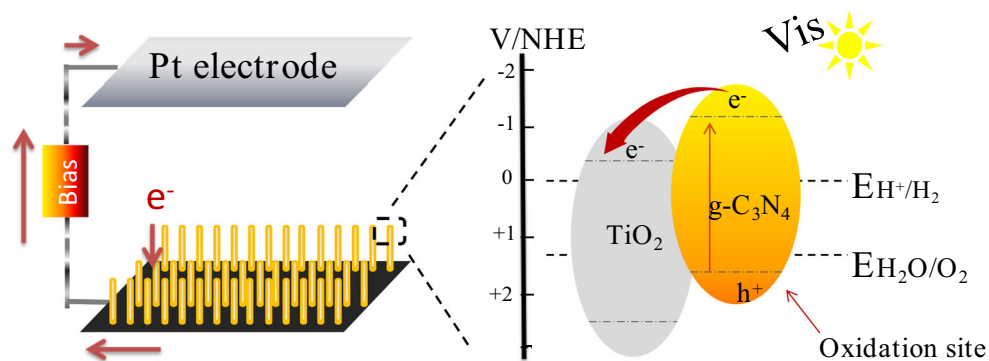


**Figure 8** Schematic diagram of the possible mechanism of the charge transfer process of the TiO<sub>2</sub>/C<sub>3</sub>N<sub>4</sub> core-shell nanowire arrays under visible light irradiation.

pathway, g-C<sub>3</sub>N<sub>4</sub> serves as a stable and environmental-friendly visible light sensitizer, and effective charge spatial separation can be achieved across the well-matched core-shell interface. The TiO<sub>2</sub>/C<sub>3</sub>N<sub>4</sub> core-shell nanowire arrays exhibit higher PC and PEC performance than TiO<sub>2</sub> nanowire arrays. The PEC performance of TiO<sub>2</sub>/C<sub>3</sub>N<sub>4</sub> core-shell nanowire arrays is enhanced by one time after C<sub>3</sub>N<sub>4</sub> modification. The enhancement of PEC BPA degradation performance of TiO<sub>2</sub> nanowire arrays after C<sub>3</sub>N<sub>4</sub> modification originates from the photoabsorption enhancement and efficient charge separation induced by the type-II band alignment. The synergetic effect between electro-oxidation and PC degradation in PEC process can further improve the degradation of BPA. Two possible degradation pathways of BPA were proposed, including dehydroxylation, cleavage of C–C bonds and oxidation. We believe that this contribution might provide a promising way to construct visible-light-driven TiO<sub>2</sub>-based heterostructure photocatalysts.

## Acknowledgements

This work is supported by the National Science Foundation of China (Grant Nos. 91645108, U1162117, 21307020), Beijing Nova Program (Grant No. Z161100004916121), Prospect Oriented Foundation of China University of Petroleum, Beijing (Grant No. QZDX-2014-02), Beijing Higher Education Young Elite Teacher Project (YETP0696), Beijing Natural Science Foundation (Grant No. 2144059) and Science Foundation of China University of Petroleum, Beijing (Grant Nos. 2462014YJRC010, C201604).

## Compliance with ethical standards

**Conflict of interest** The authors declare that there is no conflict of interest regarding the publication of this paper.

**Electronic supplementary material:** The online version of this article (<https://doi.org/10.1007/s10853-018-2368-3>) contains supplementary material, which is available to authorized users.

## References

- [1] Mills A, Hunte SL (1997) An overview of semiconductor photocatalysis. *J Photochem Photobiol A* 108:1–35
- [2] Hernández Alonso MD, Fresno SSF, Coronado JM (2009) Development of alternative photocatalysts to TiO<sub>2</sub>: challenges and opportunities. *Energy Environ Sci* 2:1231–1257
- [3] Xiao P, Lou J, Zhang H et al (2018) Enhanced visible-light-driven photocatalysis from WS<sub>2</sub> quantum dots coupled to BiOCl nanosheets: synergistic effect and mechanism insight. *Catal Sci Technol* 8:201–209
- [4] Chang S, Wang Q, Liu B, Sang Y, Liu H (2017) Hierarchical TiO<sub>2</sub> nanonetwork-porous Ti 3D hybrid photocatalysts for continuous-flow photoelectrodegradation of organic pollutants. *Catal Sci Technol* 7:524–532
- [5] Li XZ, Liu HS (2005) Development of an E-H<sub>2</sub>O<sub>2</sub>/TiO<sub>2</sub> photoelectrocatalytic oxidation system for water and wastewater treatment. *Environ Sci Technol* 39:4614–4620
- [6] Quan X, Yang S, Ruan X, Zhao H (2005) Preparation of titania nanotubes and their environmental applications as electrode. *Environ Sci Technol* 39:3770–3775
- [7] Wang Y, Zhan X, Wang F, Wang Q et al (2014) Crystalline ZnO/ZnS<sub>x</sub>Se<sub>1-x</sub> core-shell nanowire arrays for efficient visible-light photoelectrocatalysis. *J Mater Chem A* 2:18413–18419
- [8] Zaroni MVB, Sene JJ, Anderson MA (2003) Photoelectrocatalytic degradation of Remazol Brilliant Orange 3R on titanium dioxide thin-film electrodes. *J Photochem Photobiol A* 157:55–63
- [9] Wang Y, Shi R, Lin J, Zhu Y (2010) Significant photocatalytic enhancement in methylene blue degradation of TiO<sub>2</sub> photocatalysts via graphene-like carbon in situ hybridization. *Appl Catal B Environ* 100:179–183
- [10] Konstantinou IK, Albanis TA (2004) TiO<sub>2</sub>-assisted photocatalytic degradation of azo dyes in aqueous solution: kinetic and mechanistic investigations: a review. *Appl Catal B Environ* 49:1–14
- [11] Tachikawa T, Fujitsuka M, Majima T (2007) Mechanistic insight into the TiO<sub>2</sub> photocatalytic reactions: design of new photocatalysts. *J Phys Chem C* 111:5259–5275
- [12] Li H, Cheng C, Li X, Liu J, Guan C, Tay YY et al (2011) Composition-graded Zn<sub>x</sub>Cd<sub>1-x</sub>Se@ZnO core-shell nanowire array electrodes for photoelectrochemical hydrogen generation. *J Phys Chem C* 116:3802–3807
- [13] Wang Y, Wang F, He J (2013) Controlled fabrication and photocatalytic properties of a three-dimensional ZnO nanowire/reduced graphene oxide/CdS heterostructure on carbon cloth. *Nanoscale* 5:11291–11297
- [14] Cao X, Tian G, Chen Y, Zhou J, Zhou W, Tian C et al (2014) Hierarchical composites of TiO<sub>2</sub> nanowire arrays on reduced

- graphene oxide nanosheets with enhanced photocatalytic hydrogen evolution performance. *J Mater Chem A* 2:4366–4374
- [15] Wang C, Chen Z, Jin H, Cao C, Li J, Mi Z (2014) Enhancing visible-light photoelectrochemical water splitting through transition-metal doped TiO<sub>2</sub> nanorod arrays. *J Mater Chem A* 2:17820–17827
- [16] Hoang S, Berglund SP, Hahn NT, Bard AJ, Mullins CB (2012) Enhancing visible light photo-oxidation of water with TiO<sub>2</sub> nanowire arrays via cotreatment with H<sub>2</sub> and NH<sub>3</sub>: synergistic effects between Ti<sup>3+</sup> and N. *J Am Chem Soc* 134:3659–3662
- [17] Pu YC, Wang G, Chang KD, Ling Y, Lin YK, Fitzmorris BC et al (2013) Au nanostructure-decorated TiO<sub>2</sub> nanowires exhibiting photoactivity across entire UV-visible region for photoelectrochemical water splitting. *Nano Lett* 13:3817–3823
- [18] Teng W, Li X, Zhao Q, Chen G (2013) Fabrication of Ag/Ag<sub>3</sub>PO<sub>4</sub>/TiO<sub>2</sub> heterostructure photoelectrodes for efficient decomposition of 2-chlorophenol under visible light irradiation. *J Mater Chem A* 1:9060–9068
- [19] Liu S, Li H, Mo R, Chen Q, Yang S, Zhong J (2016) ZnSe sensitized and Co-Pi catalyzed TiO<sub>2</sub> nanowire array photoanode for solar-driven water splitting. *J Electrochem Soc* 163:H744–H749
- [20] Ai G, Sun W, Gao X, Zhang Y, Peng LM (2011) Hybrid CdSe/TiO<sub>2</sub> nanowire photoelectrodes: fabrication and photoelectric performance. *J Mater Chem* 21:8749–8755
- [21] Ai G, Li H, Liu S, Mo R, Zhong J (2015) Solar water splitting by TiO<sub>2</sub>/CdS/Co-Pi nanowire array photoanode enhanced with Co-Pi as hole transfer relay and CdS as light absorber. *Adv Funct Mater* 25:5706–5713
- [22] Yang H, Fan W, Vaneski A, Susha AS, Teoh WY, Rogach AL (2012) Heterojunction engineering of CdTe and CdSe quantum dots on TiO<sub>2</sub> nanotube arrays: intricate effects of size-dependency and interfacial contact on photoconversion efficiencies. *Adv Funct Mater* 22:2821–2829
- [23] Ge M, Cao C, Huang J, Li S, Chen Z, Zhang KQ et al (2016) A review of one-dimensional TiO<sub>2</sub> nanostructured materials for environmental and energy applications. *J Mater Chem A* 4:6772–6801
- [24] Mahadik MA, Shinde PS, Cho M, Jang JS (2015) Fabrication of a ternary CdS/ZnIn<sub>2</sub>S<sub>4</sub>/TiO<sub>2</sub> heterojunction for enhancing photoelectrochemical performance: effect of cascading electron-hole transfer. *J Mater Chem A* 3:23597–23606
- [25] Wang X, Maeda K, Thomas A, Takanabe K, Xin G, Carlsson JM et al (2009) A metal-free polymeric photocatalyst for hydrogen production from water under visible light. *Nat Mater* 8:76–80
- [26] Wang X, Maeda K, Chen X, Takanabe K, Domen K, Hou Y et al (2009) Polymer semiconductors for artificial photosynthesis: hydrogen evolution by mesoporous graphitic carbon nitride with visible light. *J Am Chem Soc* 131:1680–1681
- [27] Ong WJ, Tan LL, Ng YH, Yong ST, Chai SP (2016) Graphitic carbon nitride (g-C<sub>3</sub>N<sub>4</sub>)-based photocatalysts for artificial photosynthesis and environmental remediation: are we a step closer to achieving sustainability. *Chem Rev* 116:7159–7329
- [28] Wang Y, Wang X, Antonietti M (2012) Polymeric graphitic carbon nitride as a heterogeneous organocatalyst: from photochemistry to multipurpose catalysis to sustainable chemistry. *Angew Chem Int Edit* 51:68–89
- [29] Wang Y, Shi R, Lin J, Zhu Y (2011) Enhancement of photocurrent and photocatalytic activity of ZnO hybridized with graphite-like C<sub>3</sub>N<sub>4</sub>. *Energy Environ Sci* 4:2922–2929
- [30] Wang Y, Bai X, Pan C, He J, Zhu Y (2012) Enhancement of photocatalytic activity of Bi<sub>2</sub>WO<sub>6</sub> hybridized with graphite-like C<sub>3</sub>N<sub>4</sub>. *J Mater Chem* 22:11568–11573
- [31] Wang Y, Wang Z, Muhammad S, He J (2012) Graphite-like C<sub>3</sub>N<sub>4</sub> hybridized ZnWO<sub>4</sub> nanorods: synthesis and its enhanced photocatalysis in visible light. *Cryst Eng Comm* 14:5065–5070
- [32] Hao R, Wang G, Tang H, Sun L, Xu C, Han D (2016) Template-free preparation of macro/mesoporous g-C<sub>3</sub>N<sub>4</sub>/TiO<sub>2</sub> heterojunction photocatalysts with enhanced visible light photocatalytic activity. *Appl Catal B-Environ* 187:47–58
- [33] Chen X, Wei J, Hou R, Liang Y, Xie Z, Zhu Y et al (2016) Graphene-based photocatalytic composites. *Appl Catal B Environ* 188:342–350
- [34] Zhou J, Zhang M, Zhu Y (2015) Photocatalytic enhancement of hybrid C<sub>3</sub>N<sub>4</sub>/TiO<sub>2</sub> prepared via ball milling method. *Phys Chem Chem Phys* 17:3647–3652
- [35] Gu L, Wang J, Zou Z, Han X (2014) Graphitic-C<sub>3</sub>N<sub>4</sub>-hybridized TiO<sub>2</sub> nanosheets with reactive 001 facets to enhance the UV-and visible-light photocatalytic activity. *J Hazard Mater* 268:216–223
- [36] Yang L, Li Z, Jiang H, Jiang W, Su R, Luo S et al (2016) Photoelectrocatalytic oxidation of bisphenol A over mesh of TiO<sub>2</sub>/graphene/Cu<sub>2</sub>O. *Appl Catal B-Environ* 183:75–85
- [37] Xiang G, Yu Z, Hou Y, Chen Y, Peng Z, Sun L et al (2016) Simulated solar-light induced photoelectrocatalytic degradation of bisphenol-A using Fe<sup>3+</sup>-doped TiO<sub>2</sub> nanotube arrays as a photoanode with simultaneous aeration. *Sep Purif Technol* 161:144–151
- [38] Feng X, Shankar K, Varghese K, Paulose M, Latempa J, Grimes A (2008) Vertically aligned single crystal TiO<sub>2</sub> nanowire arrays grown directly on transparent conducting

- oxide coated glass: synthesis details and applications. *Nano Lett* 8:3781–3786
- [39] Cao S, Low J, Yu J, Jaroniec M (2015) Polymeric photocatalysts based on graphitic carbon nitride. *Adv Mater* 27:2150–2176
- [40] Zheng Y, Lin L, Wang B, Wang X (2015) Graphitic carbon nitride polymers toward sustainable photoredox catalysis. *Angew Chem Int Edit* 54:12868–12884
- [41] Wang XJ, Yang WY, Li FT, Xue YB, Liu RH, Hao YJ (2013) In situ microwave-assisted synthesis of porous N-TiO<sub>2</sub>/g-C<sub>3</sub>N<sub>4</sub> heterojunctions with enhanced visible-light photocatalytic properties. *Ind Eng Chem Res* 52:17140–17150
- [42] Yan SC, Li ZS, Zou ZG (2010) Photodegradation of rhodamine B and methyl orange over boron-doped g-C<sub>3</sub>N<sub>4</sub> under visible light irradiation. *Langmuir* 26:3894–3901
- [43] Ng J, Wang X, Sun D (2011) One-pot hydrothermal synthesis of a hierarchical nanofungus-like anatase TiO<sub>2</sub> thin film for photocatalytic oxidation of bisphenol A. *Appl Catal B Environ* 110:260–272
- [44] Ng J, Xu S, Zhang X, Yang H, Sun D (2010) Hybridized nanowires and cubes: a novel architecture of a heterojunctioned TiO<sub>2</sub>/SrTiO<sub>3</sub> thin film for efficient water splitting. *Adv Funct Mater* 20:4287–4294
- [45] Leng WH, Zhang Z, Zhang JQ, Cao CN (2005) Investigation of the kinetics of a TiO<sub>2</sub> photoelectrocatalytic reaction involving charge transfer and recombination through surface states by electrochemical impedance spectroscopy. *J Phys Chem B* 109:15008–15023
- [46] Wang Y, Xu J, Zong W, Zhu Y (2011) Enhancement of photoelectric catalytic activity of TiO<sub>2</sub> film via polyaniline hybridization. *J Solid State Chem* 184:1433–1438
- [47] Zhao X, Xu T, Yao W, Zhang C, Zhu Y (2007) Photoelectrocatalytic degradation of 4-chlorophenol at Bi<sub>2</sub>WO<sub>6</sub> nanoflake film electrode under visible light irradiation. *Appl Catal B-Environ* 72:92–97
- [48] Zhang T, Ding Y, Tang H (2015) Generation of singlet oxygen over Bi(V)/Bi(III) composite and its use for oxidative degradation of organic pollutants. *Chem Eng J* 264:681–689
- [49] Han Q, Wang H, Dong W, Liu T, Yin Y, Fan H (2015) Degradation of bisphenol A by ferrate (VI) oxidation: kinetics, products and toxicity assessment. *Chem Eng J* 262:34–40
- [50] Wang C, Zhu L, Wei M, Chen P, Shan G (2012) Photolytic reaction mechanism and impacts of coexisting substances on photodegradation of bisphenol A by Bi<sub>2</sub>WO<sub>6</sub> in water. *Water Res* 46:845–853
- [51] Lee H, Choi W (2002) Photocatalytic oxidation of arsenite in TiO<sub>2</sub> suspension: kinetics and mechanisms. *Environ Sci Technol* 36:3872–3878
- [52] Wang Y, Wang Q, Zhan X, Wang F, Safdar M, He J (2013) Visible light driven type II heterostructures and their enhanced photocatalysis properties: a review. *Nanoscale* 5:8326–8339